Computer Methods and Programs in Biomedicine 219 (2022) 106757

Contents lists available at ScienceDirect

Computer Methods and Programs in Biomedicine

journal homepage: www.elsevier.com/locate/cmpb

Evaluation of stent effect and thrombosis generation with different blood rheology on an intracranial aneurysm by the Lattice Boltzmann method

Farouk Mezali[a,b], Saida Benmamar[a], Khatir Naima[c], Houari Ameur[c,*], Ouared Rafik[a]

[a] Water Sciences Research laboratory: LRS-Eau, National Polytechnic School, El harrach, Algiers
[b] Hydraulics department, Faculty of Technology-BP 166 M'sila 28000 Algeria
[c] Department of Technology, University Centre of Naama (Ctr Univ Naama), P.O. Box 66, Naama 45000, Algeria

ARTICLE INFO

Article history:
Received 26 January 2022
Revised 7 March 2022
Accepted 12 March 2022

Keywords:
Lattice Boltzmann method
Stent Effect
Thrombosis generation
Blood rheology
Intracranial aneurysm
Hemodynamic

ABSTRACT

Background and objective: Treatment of intracranial aneurysms with flow-diverting stents prevents rupture by reducing blood flow and creating thrombosis within the aneurysm. This paper aims to assess the hemodynamic effect of placing stents with different struts (0, 3, 5, 7 struts) on intracranial aneurysms and to propose a simple prediction model of thrombosis zone without any further computational cost.
Method: Lattice Boltzmann method with different rheological models (Newtonian, Carreau-Yasuda, KL) of blood are used to study the hemodynamic effect of flow-diverting stents in the aneurysm. Pulsatile flow boundary conditions were applied in the inlet of the artery. The average Reynolds number was resulting Re = 111. The Lagrangian tracking of the particle was developed to assess the intra-aneurysmal blood stagnation. To predict the probable thrombose zone induced by flow-diverting stents, the shear rate threshold is utilized to determine the nodes of fluid to clot.
Results: The results show that the flow patterns into the aneurysmal sac develop a vortex, decreasing after stent placement until disappearance for the stent with seven struts (porosity 71.4%). Velocity, shear rate, shear stress, trajectory, path length, and occlusion rate are compared before and after stent placement. These parameters decrease inversely with the porosity of the stent. The three models yield a closes result of the (velocity, shear rate, occlusion rate). Tracking the fluid-particle trajectory shows that the length of the particle paths decreases with the number of struts causing fluid to slow down and increase, consequently, the residence time into the sac.
Conclusion: The flow-diverting stents placement cause the reduction of dynamic flow within aneurysm. The reduction effect is almost the same below five struts (80% of porosity). The results show that, if our objective is restricted to estimating the hemodynamic effect, measured by (velocity, shear rate, occlusion rate), the differences between rheological behavior models are, practically, not significant, and the models can be used indifferently.

1. Introduction

An intracranial aneurysm (IA) is a dilation of an artery segment located inside the skull. It affects about 2-5% of the population [1,2]. This dilation is related to the weakening of the vessel wall. Under certain conditions, the aneurysm may rupture. The rupture of the aneurysm is called subarachnoid hemorrhage (SAH), which occurs with an incidence of about 6.67 per 100,000 people/year [3]. The rupture is dangerous and may lead to death. The mortality rate caused by SAH is 27%-44% [4]. Worldwide, it is estimated that nearly 500,000 people will be affected by a SAH each year, almost two-thirds of whose are located in low- and middle-income countries [3]. Surgical and endovascular techniques have been applied for the treatment of IAs. The purpose of these techniques is to exclude the malformation of the bloodstream, avoiding the recurrence of the ruptured aneurysm. The advantage of endovascular treatment is that it does not require an open operation (craniotomy). Endovascular techniques are preferred over surgical techniques in the treatment of IAs [5].

Among the most popular endovascular techniques is embolization. It consists of inserting a fine probe, through a catheter, into the femoral artery and making it travel to the brain. Once in the aneurysm, the probe delivers a tiny platinum spring (coils) which

* Corresponding author.
E-mail addresses: mezali_farouk@yahoo.fr (F. Mezali), saida.benmamar@g.enp.edu.dz (S. Benmamar), knaima@cuniv-naama.dz (K. Naima), ameur.houari@cuniv-naama.dz (H. Ameur).

https://doi.org/10.1016/j.cmpb.2022.106757
0169-2607/

will curl on them until completely plugging the aneurysm. This leads to the rapid formation of thrombosis and aneurysm closure. Thus, the risk of rupture is eliminated. This technique is very effective [6]. However, it presents a series of limitations, especially for aneurysms with wide necks [7]. Furthermore, the treatment of IAs with a porous stent is proposed as a minimally invasive method to prevent rupture and promote thrombus formation within the aneurysm. It consists of introducing a mesh tube via the catheter into the arterial pathway to the neck of the aneurysm and then deployed to prevent blood flow from entering the aneurysm.

Since the beginning of 2008, the technological evolution of stents has made it possible to have new intracranial stents known as 'Flow Diverter: FD' or 'Flow Diverter Stent: FDS' with a tighter and denser mesh than traditional intracranial stents [5]. This dense mesh redirects blood to flow more significantly into the main artery and limits intra-aneurysm blood flow, leading to stagnation in the aneurysm sac and rapid thrombus formation. This process ends with the occlusion of the aneurysm and, as a result, its self-repair by the organism. Treatment with FD is mainly prescribed for unruptured aneurysms with complex anatomy (fusiform, dissecting, wide neck, bifurcation with side branches) where coiling and clipping are difficult or impossible [7]. The occlusion of the aneurysm occurs gradually after insertion of the stent leading to the formation of the thrombus inside the sac. From a hemodynamic point of view, the decrease of the flow velocity and the shear rate in the sac, and therefore the increase in the residence time of the blood, favors the accumulation and aggregation of platelets inside the aneurysm resulting in aneurysmal thrombus [8,9].

Several studies have been carried out on the effect of the stent in IA. A part of these studies focused on the effect of stent on hemodynamic change in IA [10,11]; other studies focused on the thrombose genesis into IA and its modelling [12,13]. Baruch et al. [11] conducted a numerical study on artificial stented aneurysms and has proven porosity's importance in reducing the intra-aneurysmal flow. Kulcsár et al. [14] conducted a numerical and experimental study on the intra-aneurismal blood flow. The results showed that complete thrombosis is produced if enough flow velocity reduction and wall shear stress occurs. Hirabayashi [15] and Hyun Kim [16] developed an approach based on the Lattice Boltzmann Method (LBM) and indicated the importance of stent design and positioning to produce more effective flow reduction. The results were based on velocity, shear rate, and viscosity. More recently, various studies proposed more or less complicated approaches to modeling clotting development into aneurysms [12,13,17]. However, a detailed investigation including the shear rate, shear stresses, velocity, fluid age, and thrombosis genesis is not extensively studied.

The main objective of this work is to investigate the blood flow inside the IA before and after the implementation of the FD and provide, with a simple approach, a quick assessment of the potential zone of blood thrombosis. Indeed, few works address the modeling of thrombosis occlusion of aneurysm by LBM. Compared to the existing literature [2,7,12], this study considers more flow parameters. These parameters are:

- The variation of the maximum velocity before and after the implementation of the FD.
- The variation of the shear rate and the shear stress.
- Individual particle path and the measurement of fluid age by Lagrangian tracking of particles seeded in selected points.
- Rate occlusion of the aneurysmal according to the number of struts (porosity stent).

Share rate, share rate stress, and fluid age control the trigger and the progression of aneurysm thrombus [9,14,18]. Consequently, they help to predict the potential zones for thrombosis formation.

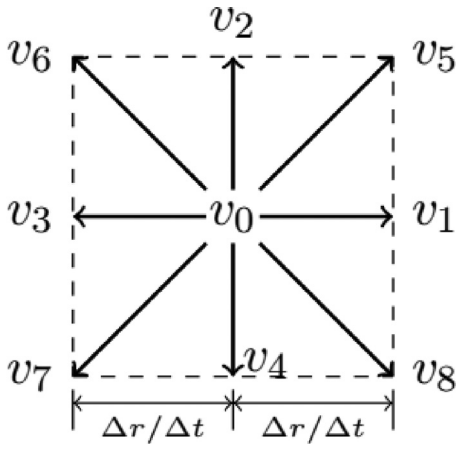

Fig. 1. Discrete velocity v_i for D2Q9, with $v_0 = (0,0)$.

The rheological behavior of the blood in the aneurysm is considered. Three models are used: Newtonian, Carreau-Yasuda, and KL.

2. Methods

2.1. Modeling approach

In this present work, the hemodynamic modeling is carried out using the Lattice Boltzmann Method (LBM). The hemodynamic analysis was conducted as follows: (i) computation of the flow fields by solving the LB equation; (ii) seeding of passive particles in the fluid; and computation of their trajectories and their travel times. This travel time is considered to be a measure of the fluid age; (iii) the previous steps (i) and (ii) were repeated with various FD porosity and different rheological behavior. The effect of changing FD is measured by comparing the extremum of the velocity, shear rate, shear stress, and fluid travel time at selected control points in the aneurysm sac.

2.1.1. The Lattice-Boltzmann Method (LBM)

The computation of the flow fields, namely velocity, shear rate, and shear stress, is performed by the lattice Boltzmann method (LBM). LBM is a numerical technique that aims to model a physical system in terms of the dynamics of the particles at the mesoscopic scale. It is currently considered an alternative to the standard methods used in CFD and has been widely used to simulate various complex fluid flows [19,20].

In this current study, the fluid is represented by the lattice-BGK (LBGK) model given by the following equation [19,21]:

$$f_i(r + \Delta t\, v_i,\ t + \Delta t) = (1/\tau) f_i^{(0)}(r,\ t) + (1 - 1/\tau) f_i(r,\ t) \qquad (1)$$

where $f_i\ (r,\ t)$ denotes the probability distribution function. This function gives the probability that a fluid particle with velocity v_i enters lattice node of r-coordinate at time t. The probable admissible velocity v_i depends on the structure of the lattice. D2Q9 lattice is used in the present study, as shown in Fig. 1. The index i varies from 0 to 8 where 8 is the number of links in the D2Q9 lattice. By convention $v_0 = 0$ and f_0 represents the density distribution of particles at rest.

The density and velocity of the fluid on a macroscopic scale are given as follows:

$$\rho = \sum_{i=0}^{8} m_i f_i \qquad (2)$$

$$\rho u = \sum_{i=0}^{8} m_i f_i v_i \qquad (3)$$

The quantities m_i denote the weights, and their values are associated with the lattice directions and depend on their dimensions. For the lattice type D2Q9, the weights can be written as [19,20]:

$$m_0 = \frac{4}{9},\ m_{1-4} = \frac{1}{9},\ m_{5-8} = \frac{1}{36} \tag{4}$$

The time step Δt of the simulation is set equal to unity [19,20]. The number τ denotes the relaxation time, and the $f_i^{(0)}$ is the local equilibrium function. The general formula of local equilibrium functions is expressed as [19,20]:

$$f_i^{(0)} = F_i^{(0)}(\rho, u) = \rho \frac{C_4}{{C_2}^2}\left[1 + \frac{v_{i\alpha}u_\alpha}{{c_s}^2} + \frac{1}{2}\left(\frac{v_{i\alpha}u_\alpha}{{c_s}^2}\right)^2 - \frac{u}{2{c_s}^2}\right],$$
$$f_0^{(0)} = F_0^{(0)}(\rho, u) = \rho\left(1 - \frac{C_0 C_4}{{C_2}^2}\right)\left(1 - \frac{u^2}{2{c_s}^2}\right) \tag{5}$$

where the index α denotes the directions of space and c_s is the speed of sound. The Einstein summation convention is used for the repeated index of space. Generally, the square of the speed of sound is chosen as ${c_s}^2 = {v_l}^2(\frac{C_4}{C_2})$ where $v_l = (\frac{\Delta r}{\Delta t})$. The C_0, C_2 and C_4 are constants linked to the structure of the lattice. For the lattice D2Q9, these constants are equal to: $C_0 = 20,\ C_2 = 12$ and $C_4 = 4$.

The nine components of the velocity v_i are given as:

$$\begin{cases} v_0 = (0,\ 0) \\ v_i = (\cos(i-1)\pi/2,\ \sin(i-1)\pi/2)\Delta x/\Delta t,\ i = 1-4 \\ v_i = (\cos(2i-9)\pi/4,\ \sin(2i-9)\pi/4)\Delta x/\Delta t,\ i = 5-8 \end{cases} \tag{6}$$

Eq. (1) is usually implemented in two steps:

$$\text{Propagation}: \tilde{f}_i(r + \Delta t v_i, t + \Delta t) = f_i(r, t)$$

$$\text{Collision}: f_i(r,t) = \tilde{f}_i(r,t) - \frac{1}{\tau}\left[\tilde{f}_i(r,t) - f_i^{(0)}(r,t)\right]$$

Using asymptotic analysis, it can be shown that Eq. (1), which represents the dynamics of fluid particles on the mesoscopic scale, can reproduce the equations of Navier-Stokes [20]:

$$\partial_t \rho + \rho \nabla.\mathbf{u} = 0,$$
$$\partial_t u + \mathbf{u}.\nabla.\mathbf{u} = -\nabla p + \nu \nabla^2 \mathbf{u}, \tag{7}$$

It can also be shown that the pressure is related to density by equation $p = c_s^2 \rho$ and the kinematic viscosity [19,20] through:

$$\nu = \Delta t\ {v_l}^2 \frac{C_4}{C_2}\left(\tau - \frac{1}{2}\right) \tag{8}$$

and in the case D2Q9, the speed of sound is $c_s = (1/\sqrt{3})v_l$ and the viscosity $\nu = \frac{1}{3}(\tau - \frac{1}{2}){v_l}^2 \Delta t$.

2.1.2. Rheological models of blood

The composition and structure of blood are responsible for its rheological behavior. Blood is made up of a liquid called plasma and suspended particles: erythrocytes, so-called red blood cells (RBCs), leukocytes or white blood cells, and platelets. The behavior of RBCs is a function of the shear rate, which is at the origin of the shear-thinning character of blood [22,23]. Thus, the rheological properties of blood can significantly affect flow dynamics, especially in slow flow zones [24,25].

The flow through the aneurysm is slower than the flow through the parent artery, especially when the stent is placed in the neck of the aneurysm where the blood stagnates for a significant period.

For shear-thinning fluids, the dynamic viscosity μ is not constant, and it is a decreasing function of the magnitude of shear rate $\dot{\gamma}$. The relation expresses the stress tensor is:

$$\sigma = 2\mu(\dot{\gamma}) * S \tag{9}$$

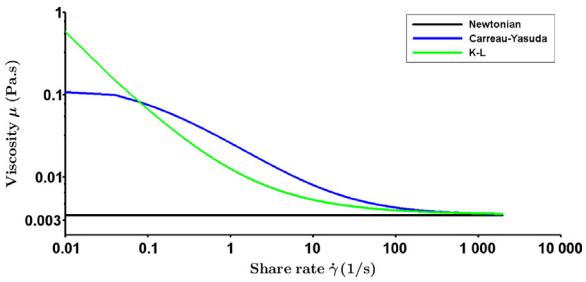

Fig. 2. Dynamic viscosity for the three models (Newtonian, C-Y et KL) according to the magnitude of shear rate.

In the commonly used language of LBM, the magnitude of shear rate $\dot{\gamma}$ is usually denoted $|S|$. It is given by [20,21,26]:

$$\dot{\gamma} = |S| = \sqrt{2S_{\alpha\beta}S_{\alpha\beta}} \tag{10}$$

with α and β denotes the coordinates direction. $|S|$ is also called rate of strain matrix magnitude'. The rate of deformation matrix $S_{\alpha\beta}$ defined by:

$$S_{\alpha\beta} = 1/2\left(\partial_\alpha u_\beta + \partial_\beta u_\alpha\right) \tag{11}$$

Different rheological models of blood have been proposed in the literature [22,27,28]. Usually, shear-thinning blood viscosity models are classified into three categories [29]: Casson models, Carreau models, and Power models. Two models: K-L model (Casson type) and the Carreau-Yasuda model are treated.

K-L Model [29,30]: the dynamic viscosity is given by:

$$\mu(\dot{\gamma}) = \frac{1}{\dot{\gamma}}\left[\tau_c + \mu_c\left(\alpha_2\sqrt{\dot{\gamma}} + \alpha_1\dot{\gamma}\right)\right], \text{ where } \mu_c = 0.0035,$$
$$\tau_c = 0.005,\ \alpha_1 = 1,\ \alpha_2 = 1.19523.$$

The K-L model is an improved modification and extended of the basic Casson model [29]. It was first proposed by [30], they concluded that the model explains well the rheofluidizing behavior of blood, in a wide range of shear rates, better than the Newtonian and Casson models. In the K-L model, the parameters μ_c and τ_c are related to hematocrit, volume of red blood cells per volume of whole blood [30,31].

Carreau-Yasuda model [22,32,33]**:** the second model used is the model of Carreau-Yasuda

$$\frac{\mu(\dot{\gamma}) - \mu_\infty}{\mu_\infty - \mu_0} = \left(1 - (\lambda\dot{\gamma}^a\right)^{(n-1)/a},\ \mu_0 = 0.056\,Pas,$$
$$\mu_\infty = 0.00345\,Pas,\ \lambda = 1.902s,\ n = 0.22,\ a = 1.25$$

The different parameters of the model are, at the base, fitted to experimental data, where λ is the relaxation time constant, μ_0 is the viscosity at a very low magnitude of shear rate $\dot{\gamma}$, μ_∞ is the viscosity when $\dot{\gamma}$ tends to very high value, n is the power-law index, a denotes the width of the transition region between Newtonian and power-law behavior. This model has two Newtonian plateaus, and the model resembles Newtonian behavior. The first plateau, at high shear rates above 100 s^{-1}, viscosity of CY model is very close to that of the Newton model. The second Newtonian plateau is manifested at low shear rates. The C-Y model's main advantage compared to the K-L model is the continuity of the function near zero, making its programming easier than the K-L model Fig. 2. shows a log-log plot of the dynamic viscosity versus shear rate for the models selected in our study.

The rheological model of Newtonian fluid is characterized by a constant viscosity and its independence to the shear rate [27]. The constitutive Eq. (9) becomes linear: $\sigma = 2\mu^* S$.

For the non-Newtonian fluid, the dependence of the viscosity on the shear rate magnitude slightly modifies the calculations performed by the LBM.

The tensor $S_{\alpha\beta}$ can be calculated locally without passing by the operations of derivation. Indeed [20,21]:

$$S_{\alpha\beta} = -\frac{3}{2\rho\tau\Delta t}\sum_{i=0}^{8} v_{i\alpha}v_{i\beta}\left(f_i - f_i^{(0)}\right) = -\frac{3}{2\rho\tau\Delta t}\Pi_{\alpha\beta}^{(1)} \tag{12}$$

and

$$\Pi_{\alpha\beta}^{(1)} = \sum_{i=0}^{8} v_{i\alpha}v_{i\beta}\left(f_i - f_i^{(0)}\right) \tag{13}$$

Using Eqs. (12) and (13), the magnitude of shear rate can be written:

$$|S| = \sqrt{2S_{\alpha\beta}S_{\alpha\beta}} = \frac{3}{\rho\tau\Delta t}\sqrt{\Pi_{\alpha\beta}^{(1)}\Pi_{\alpha\beta}^{(1)}} \tag{14}$$

$\Pi_{\alpha\beta}^{(1)}$ is directly calculated from the distribution functions f_i Eq. (1). may be written as: $|S| = \frac{C}{\tau}$ with $C = \frac{3\sqrt{\Pi_{\alpha\beta}^{(1)}\Pi_{\alpha\beta}^{(1)}}}{\rho\Delta t}$. From the relation which gives the kinematic viscosity $\nu = \frac{1}{3}(\tau - \frac{1}{2})v_l{}^2\Delta t$ and considering the relations of rheology behavior which gives the dynamic viscosity versus shear rate, which leads to an implicit nonlinear equation $\mu(|S|) = \mu(\frac{C}{\tau})$ as a function of τ. This equation is solved by the fixed-point iteration method. The convergence is usually obtained after a few iterations. In the case of non-Newtonian behavior, the viscosity is computed at each node in the domain, which results in additional calculation run time.

2.1.3. Boundary conditions

On the walls of the blood vessel, the non-slip condition was applied. It was achieved by using the full way bounce-back condition. Indeed, the velocity of the fluid is equal to the velocity of the walls. The elasticity of the wall was not taken into account. In addition, the walls are assumed to be stationary, so one has: $u(x = x_p) = u_p = 0$ where $u(x = x_p)$ is the fluid velocity at the walls, and up is the wall velocity. The bounce-back condition consists of returning to the fluid; after the propagation step, the particle arrives towards the solid boundary. The velocity vector of all the fluid densities is inverted, so all the fluid densities will be returned to the node where they were before the last propagation step, but with an opposite velocity vector: $f_i = \tilde{f}_{\bar{i}}$ with $i = 1$, .., 8 and $\bar{i}$ is the direction opposite to i. Thus, the velocity at the wall is equal to zero. At the vessel's entrance, a Dirichlet condition on the velocity is applied. This velocity is variable over time and takes the form of a periodic wave. In the outflow boundary, the zero normal shear stress condition (ZNS) is implemented: $(-pI + 2\nu S)n = 0$. To realize this condition in term of LBM, referring to author [34], the unknown distributions f_a is expressed as:

$$f_a(N_x, j) = F_i^{(0)}(1, u) + O\left(h^2\right) \approx F_i^{(0)}(1, 0),\ \left(a = 3, 6, 7;\ j = 1,\ N_y\right) \tag{15}$$

where N_x and N_y are the subdivisions in the x and y-direction, respectively.

As for the initial condition, a zero-velocity field is imposed at time t = 0. After 30000 iterations, the solution converges on the physical solution.

2.1.4. Particle tracking and travel time

Generally, two approaches are used to calculate particle residence time (PRT): Lagrangian and Eulerian approaches [9,35,36]. The authors [9,36] used an Eulerian method that introduces an additional equation of advection of residence time. This equation models a passive scalar injected into a specific location in the flow domain. This method is more straightforward than the Lagrangian methods [9,35,36]. Unlike the Lagrangian approach, which requires a high computational cost, the Eulerian method is generally more straightforward and gives the PRT at each computation node.

In this work, the motion of small particles (platelets) is considered as the motion of passive particles. This means that the particles are advected by the velocity field as tracers, without the intervention of any force (flotation, weight, etc.) and without undergoing any chemical reaction. These assumptions lead to consider that the platelets follow the trajectories of the fluid particles. If x is the position vector of the blood platelet considered at time t, then its motion is given by the first differential equation [37]:

$$\frac{dx}{dt} = u(x, t) \tag{16}$$

For calculating the trajectories of particles seeded into fluid, one has to solve, by the explicit Euler method, the Eq. (16) after calculating the flow field by equations (2). In the first iterations, the results oscillate in a non-physical way, which is why the particles were sown at iteration 30,000 where the results stabilize, and an established regime is reached. The cardiac cycle's periodic nature and the laminar flow regime give the flow a permanent periodicity throughout the whole domain and generate streamlines that oscillate periodically and maintain constancy of shape over time. This led us to seed 70 particles at the time (t = 30,000 iterations) and perform a Lagrangian tracking for them over calculus. These particles are divided into two groups: 10 sown just after input of the vessel, and the remaining 60 are sown in different places in the aneurysm sac.

2.1.5. Path length and travel time

First, the particle travel time (t_{tr}) is introduced, it defined as follow:

$$(t_{tr})_j = \sum_{itérations,i} \Delta t_i \tag{17}$$

where $(t_{tr})_j$ is the travel time of particle j. The index i represents the iteration overtime calculated from the moment of the particles seeding. Δt_i is the time step used in the calculation. In the LBM, the time step is chosen to equal the unit. The travel time is then expressed in terms of the number of iterations.

The seeded particles begin their movements with a travel time t_{tr} equal to zero, and as they advance, this time is increased by the quantity Δt_i . If a particle point outside the computational domain, its t_{tr}stops at that instant.

The measurement of travel time t_{tr} gives an idea of the age of the fluid, but it cannot determine whether the fluid is stagnant or not. To know whether the platelets are stagnant, the path length l_{pl} is defined as:

$$\left(l_{pl}\right)_j = \sum_{itérations,i} \Delta l_i = \sum_{itérations,i} \Delta t_i\, u_j \tag{18}$$

where$(l_{pl})_j$ represents the path length accomplished by particle j during the time Δt_i . The parameter u_j represents the speed of the particle j.

2.1.6. Quickly prediction of thrombose

The model considered in this study consists of assuming that if the shear rate at a given point drops below a 'threshold' value γ_{min}, then it coagulates and becomes solid. Indeed, the lowering of the shear rate can cause thrombosis formation in the vicinity of the blood vessel wall. Generally, two parameters are taken into account to predict and model the formation and the progression of thrombose: the residence time of fluid, also called: reaction time, and the shear rate [9,12]. In the simplified model presented here, it is considered that if the shear rate is sufficiently low, then causing the fluid to slow down and exceed the temporal threshold of thrombosis. Thus, the shear rate is the only remaining criterion to trigger and rule the thrombosis.

Table 1
Dimensions of aneurysm.

D	d	h	L	Form factor (aspect ratio AR = h/d)
33 (2.60 mm)	49 (3.86 mm)	56 (4.42 mm)	345 (27.2mm)	1.14

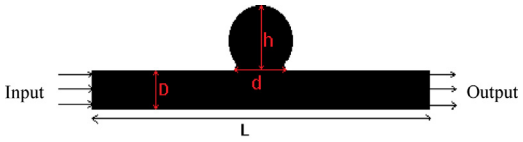

Fig. 3. Geometry (simplified) of saccular intracranial aneurysm.

Table 2
Parameters of stents for the simulation.

Stents parameters (lattice unit)				
Model of stent: n	l_s	e_s	S_p	$P = \frac{d-(n*e_s)}{d}$ %
Case 1: 0 strut	-	2	-	100 High Porosity
Case 2: 3 struts	193	2	21	88 Medium porosity
Case 3: 5 struts	193	2	10	80 Fairly low Porosity
Case 4: 7 struts	193	2	6	71.4 Low porosity

The development of thrombosis must begin from the wall to the hollow space in the sac, hence the fluid node, before being solidified, must be located in the neighboring solid node [36,38,39].

At the level of the calculation code, this is done by defining an index that takes two values: 1 and 0. If the shear rate value falls below the threshold, the indicator passes from the value 1 to the value 0, the shape of the computation domain is not fixed and evolves with each step iteration.

2.2. Computational domain

2.2.1. Geometric parameters

The case of saccular intracranial aneurysm (sIA) with and without stents is studied. This type of saccular aneurysm is found at the base in the brain, also called saccular cerebral aneurysm, and represents the majority of common types of aneurysms [40].

A simplified geometric shape was used to represent the aneurysm. The length of artery L = 345 in lattice unit (lu) and 27.2 mm in physical unit (Fig. 3). The mesh size of our whole lattice is 345 × 90. In the study of [41] the average size of the ruptured IAs is 5.3 + 3.1 mm, and the average aspect ratio is (AR = 1.66 +0.76). Therefore, and by combining a medical image that was at our disposal, so the characteristic dimensions of the aneurysm are taken as follows: the diameter of the neck d = 49 lu (3.86 mm), the depth of the sac h = 56 lu (4.42 mm) and the diameter of the main vessel D = 33 lu (2.60 mm).

Three types of stents were considered, stent with three, five and seven struts. All of the three stents have a constant length ($\boldsymbol{l_s}$ = 193 lu). The spacing $S_{\boldsymbol{p}}$ between the struts is respectively 21, 10, 6 (lu). The struts used have a square shape with a thickness e_s = 2 lu. Table 1 and Table 2 summarize the parameters of the stents used for each case.

The porosity is calculated by the relation $P = \frac{d-(n*e_s)}{d}$ with P the porosity; d = 49 the diameter of the neck; e_s the thickness of the stent wire; l_s the length of the aneurysm; S_p the spacing between the struts and n the number of struts. Fig. 4 (a-d) illustrates the four configurations considered for the simulations.

2.2.2. Physical parameters of flow

The heartbeat produces a pulsed and periodic flow of blood in the body. In [42], there are several experimental data relating to IA. The necessary data are chosen for the anterior cerebral artery. Thus, the velocity profile imposed at the input of the artery is expressed by the polynomial function:

$$V(t) = 0{,}118 + 0.228{*}t - 4.839{*}t^2 + 159.776{*}t^3 - 1962.818{*}t^4 + 11469.183{*}t^5 - 37177.801{*}t^6 + 70884.873{*}t^7 - 79225.260{*}t^8 + 48082.556{*}t^9 - 12242.977{*}t^{10}$$

This function shown in Fig. 5 will be imposed on the input of the artery.

For blood rheology, the blood is treated as a Newtonian fluid, assuming that the viscosity is constant independently of the shear rate and then as a non-Newtonian fluid using the K-L and Carreau-Yasuda models described above.

The parameter $\boldsymbol{v_l}$ which represents the ratio between the space step and the time step (Fig. 1) is chosen equal to 100. The Reynold number is calculated by considering the following three quantities: i) the maximum value of the speed $\boldsymbol{v_{max}}$ = 0.141m/s, ii) the diameter of the inlet section of the artery d = 2.61mm and iii) the dynamic viscosity $\mu = 0.0035\ kg.m^{-1}.s^{-1}$ with the density of the blood $\rho = 1055 kg/m^3$. Thus, the average Reynolds number is $Re = \frac{v_{max}\, d}{\mu/\rho} = 111.0$. Numerical scheme of LBM has an explicit numerical scheme, for this reason, the time step is habitually very small to ensure stability scheme ($\Delta t = 5.6 \times 10^{-6} s$, 1000000 steps to $t = 5.6 s$).

3. Results

In the current study, the authors developed a script code using Fortran and Python to implement blood flow behavior in aneurysm with LBM. This section presents the results obtained. First, to assess the overall quality of our numerical results, one has compared them to those obtained via the 'Ansys Fluent' calculation code. The comparison was made for a constant blood flow on the input. The systolic velocity is imposed as a condition for the input domain v_{in} = 0.141m/s. As seen in Fig. 6(a and b), the velocity field results are almost identical between the two solvers.

Two cases of saccular aneurysms of the anterior cerebral artery were considered: the aneurysm without flow diverter stent (FDS) and aneurysm with FDS. Fig. 7(a-c) shows the velocity field and the streamlines for the three rheological models: Newtonian, K-L, and Carreau-Yasuda.

3.1. Streamline

Figs. 7(a.1-a.4) correspond to the Newtonian rheological model. Fig. 7(a.1) shows a stent-free aneurysm where a clearly defined vortex is present in the aneurysm sac. It is noted that the vortex's size decreases with the stent's porosity. Also, this vortex moves to the left and tends to disappear when the porosity decreases.

Figs. 7(b.1-b.4) show the velocity field and the streamlines for the rheological model of Carreau-Yasuda. The overall appearance of the results is the same as that of the Newtonian fluid hypothesis. Indeed, a large recirculation Rouleau is present in the aneurysm sac without a stent.

For the K-L model, the same remarks are made, except for the decreases of the vortex intensity. Indeed, the vortex tends to disappear from the case of the stent with five struts.

It can also be seen, from Figs. 7, that the particles at the pores of the stent enter the aneurysm sac slightly and pass to the main artery. The particles just above the pores make their trajectories completely in the sac.

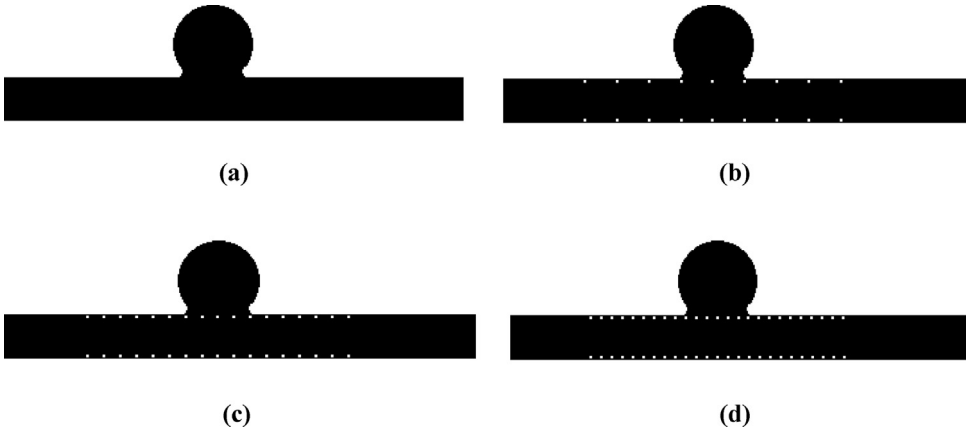

Fig. 4. (a) Saccular intracranial aneurysm without stent; (b) stent with 3 struts; (c) stent with 5 struts; (d) stent with 7 struts.

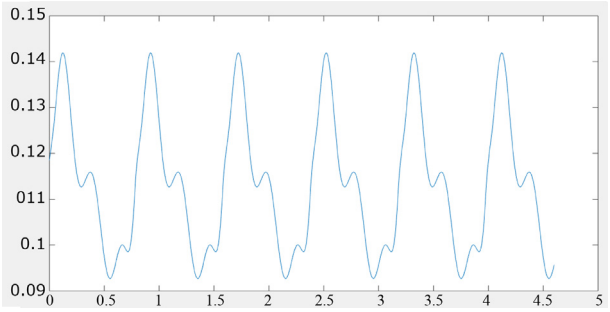

Fig. 5. Curve of periodic pulsed velocity in the anterior cerebral artery.

The complex aneurysmal flow and its dynamics will be quantified in a second step. For this aim, a horizontal control line is set in the sac that collects the desired properties. The control line is defined by the two coordinate points ($x_1 = 128$, $y_1 = 52$ and $x_2 = 185$, $y_2 = 52$). The maximum values are recorded in this line for the following hemodynamic parameters: shear rate, shear stress, and velocity.

Table 3 show the change of intra-aneurysmal velocity before and after stent placement for a different number of strut and different rheological behavior. Table 4 present the change of velocity in the parent artery. It illustrates the minim-influence of the stent on the main flow.

3.2. The velocity

Table 3 indicates that the velocity decreases after placing a stent when the number of struts increases. The same remark applies to the other hemodynamic quantities: shear rate and shear

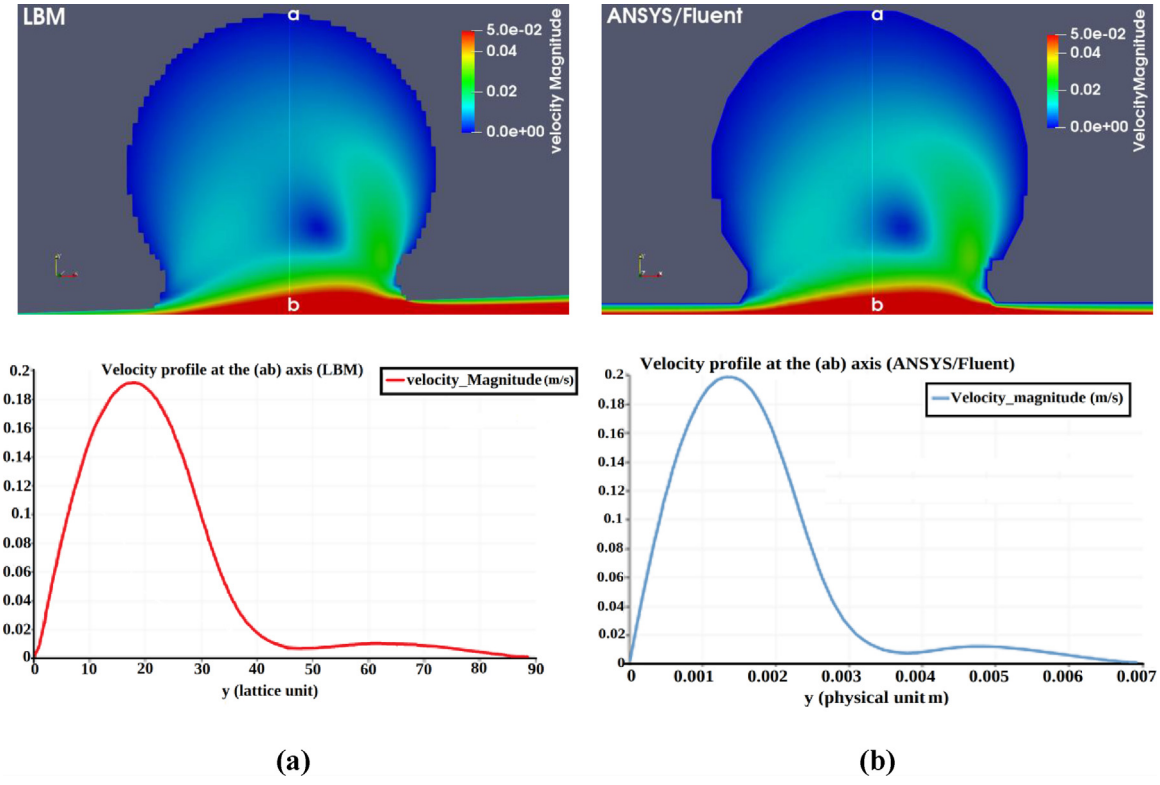

Fig. 6. Comparison of the intra-aneurysmal velocity between (a) our code and (b) fluent Ansys.

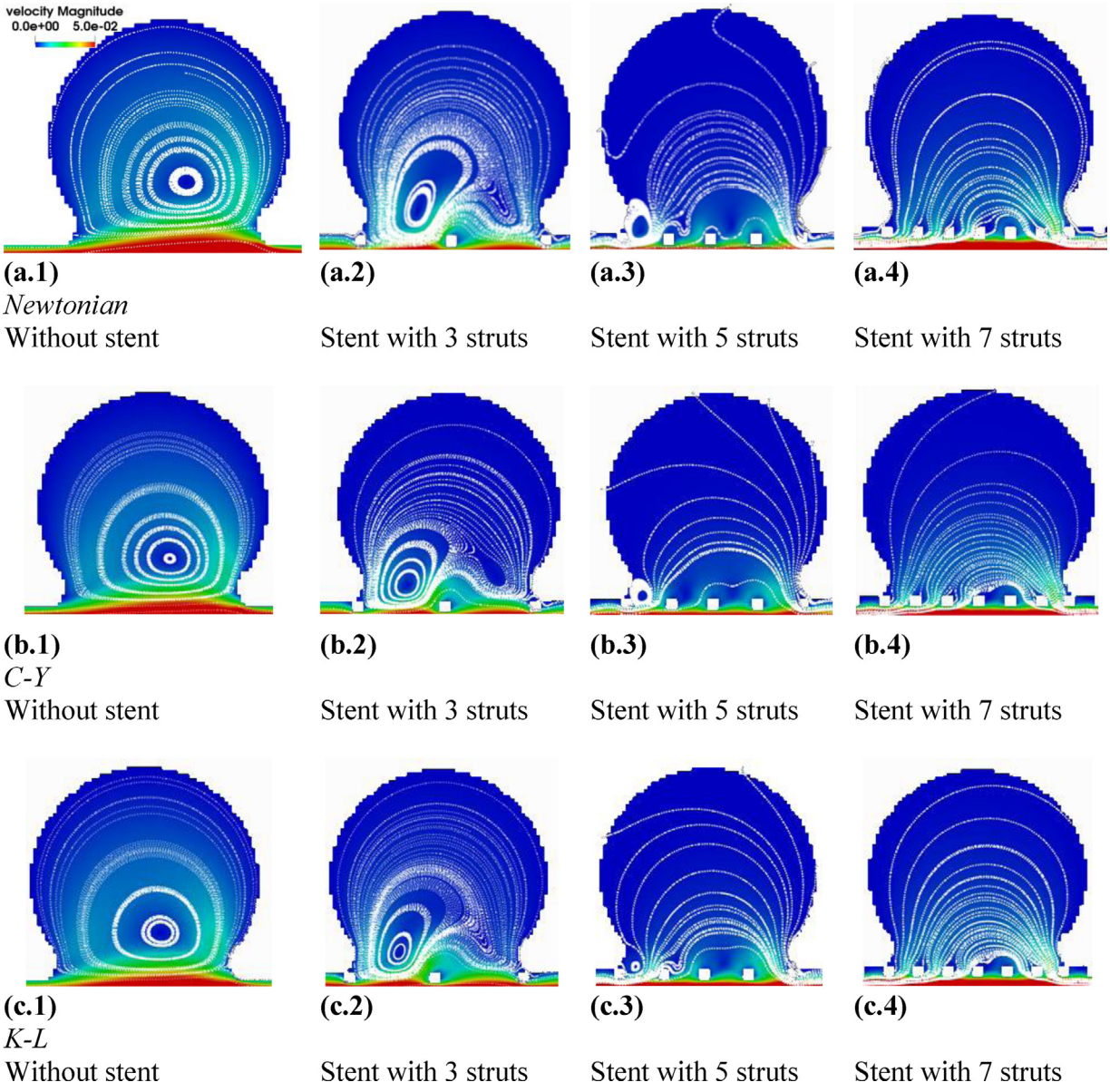

Fig. 7. Velocity field and stream lines for three rheological models with different porosities stents.

Table 3
The maximum velocity according to number of struts and rheological behavior on the control line ($x_1 = 120$, $y_1 = 5$; $x_2 = 120$, $y_2 = 35$) inside the sac of aneurysm.

	Without stent (m/s)	3 struts (m/s)	5 struts (m/s)	7 struts (m/s)
Newtonian	0.01942	0.00778	0.0038585	0.004095
C-Y	0.014376	0.00475	0.00409	0.004096
K-L	0.017635	0.00671	0.004565	0.004365

Table 4
The maximum velocity according to number of struts and rheological behavior on the control line ($x_1 = 120$, $y_1 = 5$; $x_2 = 120$, $y_2 = 35$) within parent artery before the sac of aneurysm.

	Without stent (m/s)	3 struts (m/s)	5 struts (m/s)	7 struts (m/s)
Newtonian	0.197	0.220	0.230	0.234
C-Y	0.193	0.217	0.227	0.231
K-L	0.197	0.220	0.231	0.235

Table 5
The maximum value of the shear rate obtained in the sac of aneurysm for the three rheological models.

	Without stent (s^{-1})	3 struts (s^{-1})	5 struts (s^{-1})	7 struts (s^{-1})
Newtonian	37.4	15.5323	9.1936	9.05
C-Y	28.1742	13.5000	9.6000	9.16
K-L	36.000	14.345	10.62	9.822

Table 6
The maximum shear stress value obtained in the aneurysm sac for the three rheological models.

	Without stent($kg.m^{-1}.s^{-2}$)	3 struts($kg.m^{-1}.s^{-2}$)	5 struts($kg.m^{-1}.s^{-2}$)	7 struts($kg.m^{-1}.s^{-2}$)
Newtonian	1.9363e-2	8.39917e-3	4.8214e-3	4.7180e-3
C-Y	2.3838e-2	1.463653e-2	1.20509e-2	1.174289e-2
K-L	2.4528e-2	1.1903e-2	8.5928e-3	8.031656e-3

stress, Tables 5 and 6. The maximum velocity is 0.01942 for the aneurysm without stent (high porosity) and decreases to 0.003858 for the stent of five struts (relatively low porosity). For the stent of three struts, the maximum velocity is lower about 60 % than without stent. It drops to 80.1% with five struts and 78.9% for the case of seven struts (low porosity).

Table 3 shows that the Carreau-Yasuda model gives relatively the same finding as the Newtonian model. The maximum velocity CY model decreases from 0.014376 for the aneurysm without stent to a value of 0.00409 in the aneurysm with five and seven struts, so a drop of 71.5%. The difference with the Newtonian model is 26%, 38.8%, 15.6%, and 0.02% for the cases of zero strut, three struts, five struts, and seven struts, respectively.

The same remark can also be made for the K-L model, the maximum velocity decreases from 0.017635 for the non-stent case and up to 0.004365 in the case of stent with seven struts, namely, a reduction of 75.2% is observed. These values differ 6.6% to 18.3%) from the values recorded in the Newtonian model.

3.3. The Shear rate

Table 5 shows the maximum shear rate and its reduction rate at the control points inside the aneurysm sac for different porosities and rheological behavior of the blood. The maximum value is decreased by 58.5% in the case of three struts and it decreased by (75.4% and 75.8%) in the case of five and seven struts. The C-Y and K-L models generally give the same proportions of reduction. In sum, as the porosity of the stents decreases, a reduction is observed in the shear rate for the three rheological behaviors.

3.4. The Shear stress

The causes of cerebral aneurysms are multiple; however, their growth, rupture, and thrombosis are strongly correlated with hemodynamic stresses [10,43]. This section focuses on the shear stress magnitudes and its variation by the interposition of a stent at the neck of the aneurysm. Table 6 shows the maximum shear stress.

Figs. 8(b-c-d) show the maximum magnitudes (velocity, shear rate, shear stress) in the aneurysm sac for velocity field distribution, the shear rate and the shear stress in the aneurysmal sac according to the number of struts (porosity) and the rheological behavior of the blood.

Fig. 8(a) compares the maximum velocity in the parent artery. The maximum is taken on the control line ($x_1 = 128$, $y_1 = 52$ and $x_2 = 185$, $y_2 = 52$). This line is just above the stent within the aneurysm sac. For the parent artery, the control line ($x_1 = 120$, $y_1 = 5$ and $x_2 = 120$, $y_2 = 35$) is located before the aneurysm sac.

3.5. Trajectories of fluid particles

The second set of stent effect analyses is based on the trajectories of the fluid particles in the aneurysm sac. Five points were chosen in the zone around the neck, as shown in Fig. 9. The selected positions, in principle, allow seeing the influence and interaction of the main flow in the parent artery with the flow in the sac of the aneurysm. The trajectory enables to follow the detail of the path of the particle. Fig. 9(b) shows the trajectory of the particles in the case without a stent. The paths given by the three rheological models are similar. For the stent of three struts Fig. 9(c), the particles located in the left of the neck follow a closed path, forming a less pronounced vortex than without stent, leading to the same remarks made in the discussion of streamlines. If the trajectories above the chosen points are followed, the trajectories are similar between the three rheological models, with a slight difference in the length of the path. Fig. 9(d) shows the case of a stent with five struts, one can see a sharp decrease in the vortex size while it localized to the far left of the neck. This vortex disappears completely for stents with seven struts.

3.6. Path length

The path length is the distance of trajectory accomplished by the particle fluid and the aneurysm sac in a given time. It serves to provide an idea of the age of the fluid and its degree of stagnation. For this purpose, three control points Pt_k, k = 1,2,3, are selected in the aneurysm, as shown in Fig. 10. Like mentioned in section (2.1.5), $(l_{pl})_{Pt_k}$ denote the path length of point Pt_k . It is calculated by resolution of differential Eq. (16) after collision-propagation step (Eq. 1) like explained in section (2.1.4):

$$\left(l_{pl}\right)_{Pt_k} = \sum_{itérations,i} \Delta l_i = \sum_{itérations,i} \Delta t_i \, u_{Pt_k}$$

As can be observed from Fig. 11, the Newtonian model overestimates the path length compared to the K-L and C-Y models. The K-L model is closer to the Newtonian model than the C-Y model.

3.7. Thrombose occlusion

Fig. 12 shows the occlusion rate of the aneurysm according to the number of struts and rheological behavior. The figure pointed out the formation and development of thrombosis as a function of iteration steps. The threshold $\gamma_{min} = 4s^{-1}$. The occlusion rate is close between the CY and Newtonian rheological models for the aneurysm stented. The difference is between (2.5-8%) for stented aneurysms and differs by (7-10%) from the KL and Newtonian models. The values of occlusion rate are close between the aneurysm with five and seven struts stent. The same observation is made with the hemodynamic parameters seen previously.

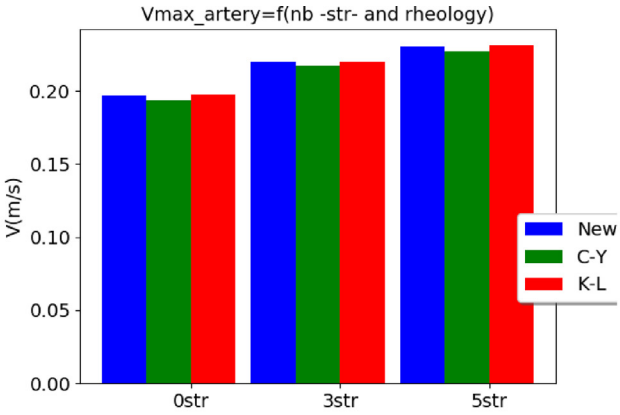

(a) Maximum velocity in the parent artery.

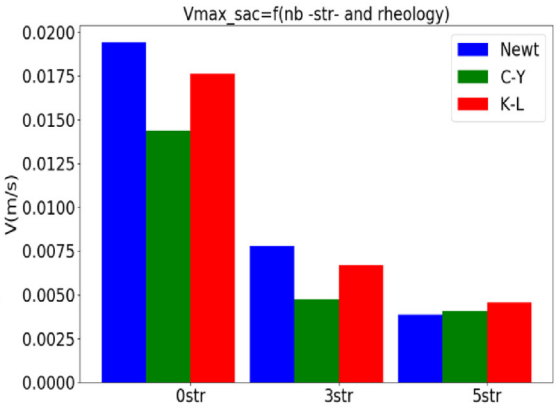

(b) Maximum velocity in the aneurysmal sac.

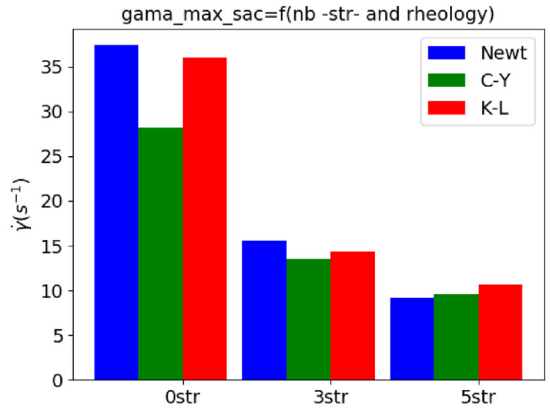

(c) Maximum shear rate in the aneurysmal sac.

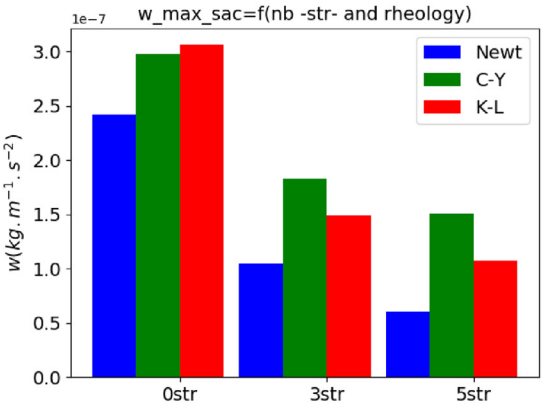

(d) Maximum shear stress in the aneurysmal sac.

Fig. 8. Comparison of the maximum magnitudes (velocity, shear rate, shear stress) in the aneurysm sac for cases b, c, and d at the control line ($x_1 = 128$, $y_1 = 52$ and $x_2 = 185$, $y_2 = 52$). At sub-figure a, the maximum velocity in the parent vessel.

Fig. 13 shows the thrombose progression according to the number of struts, predicted with the Newtonian model. In sub-Fig. 13(a), the generation of thrombose is observed without any stent. This case can be observed in some practices cases [10,44].

4. Discussion

The paper presents comparisons of several hemodynamic flow parameters (velocity, shear rate, shear stress, trajectory of particles fluid, Path length) of aneurysm with stent and without stent regardless of thrombosis. In the last part, the consequence of stent in terms of thrombosis genesis is considered. Firstly, results show a stable vortex for the streamline, resulting in stasis in the sac, commonly observed in many intracranial aneurysms [43]. The flow in the parent vessel directly generates this vortex without any obstacle.

The struts provide a physical barrier that prevents blood flux from moving freely in the sac through the neck of the aneurysm. The same observations are reported [15,45] in their numerical and experimental results and by [10] in their numerical investigation.

The intensity of this recirculating Rouleau decreases with the number of struts. For the stent of five struts, small swirls around the struts on the left side of the stent are observed. The vortex disappears in the case of seven struts.

Regarding velocity, it is low enough at the vortex center for the aneurysm without stent. For stented aneurysms, the velocity inside the sac is large around and after the struts. It decreases through the interior of the sac and tends to zero in walls.

As the fluid in the main artery moves much faster than the fluid in the aneurysm, their velocity does not change significantly between the three rheological behaviors, as shown in Table 4. This is in good agreement with the results and conclusions reported by [46,47]. Also, it is noted that the velocity in the parent artery increases slightly with the number of struts. Indeed, in the presence of the stent, the fluid escapes less through the pores of the stents into the aneurysmal sac by borrowing the main channel. The total fluid flow section is then found somewhat reduced due to the effect of the stent leading to a slight acceleration of the blood.

Table 3 suggests that the reduction in velocity beyond the third case -5 struts- is insignificant. It is noted that the decrease in porosity is not of great interest to increase the efficiency of blood stagnation in the aneurysm and consequently its thrombosis and stabilization.

For the shear stress parameters, in general, it is noticed that the reduction rate for stents with (five and seven) struts is same (New:

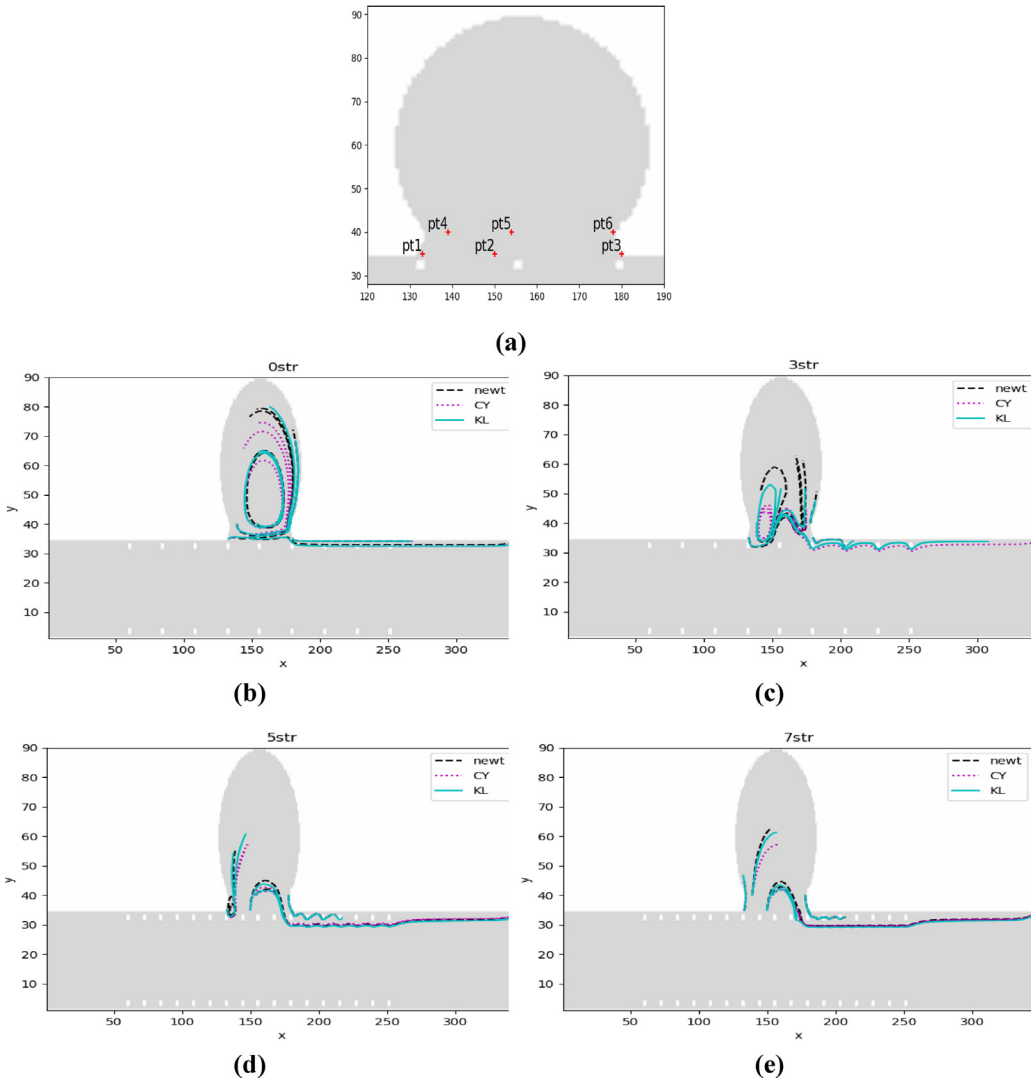

Fig. 9. Trajectories of particles fluids according to rheological behavior.

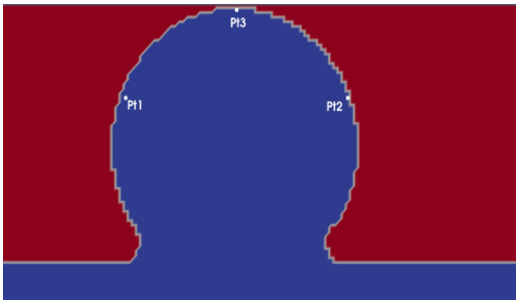

Fig. 10. The three control points selected.

75.1, 75.6%, CY: 49.4, 50.7%, KL: 65.0, 67.3%). The non-Newtonian models (C-Y and K-L) predict shear stress values higher than those given by the Newtonian model [48]. These results are explained by the fact that in the fields of low shear rates ($< 100s^{-1}$) the apparent viscosity of the blood is greater than the Newtonian viscosity, where the major parts of the blood constituents, the red blood cells, aggregate and form 'Rouleau' [26,49], the non-Newtonian effect is not negligible in these zones.

One can say that the two flows are separated and do not mix, there is no renewal of the flow in the aneurysm, and a vortex occurs due to friction between the fluid layers. This non-renewal of the flow, which leads to an increase in the fluid's age may explain the onset of thrombosis in some cases of aneurysms without a stent [44,50].

Fig. 9 shows that the size of the vortex and the length of the particle paths decrease with the number of struts, and each time the fluid reaches the upper part of the aneurysm, it slows down further, allowing a longer residence time into the sac. This may explain the observation in real cases that the clot in the aneurysm has an onion structure. The thrombosis formation occurs in successive layers, from the upper layers of the sac [38,39,51].

The difference of length path given by the K-L and Newtonian model is 2.02% to 88.6. This difference is 68.9% to 690% between the C-Y and Newtonian model. These differences obtained between the models suggest that non-Newtonian rheological models are imperative if one wants to envisage -only- the study of the hemodynamic aspect of the flow in aneurysms where the velocities and the shear rates are low. For all studied models, the reduction in path length due to the stent with three struts is between 50% and 93.8%, while for the stent with five struts. This reduction is between 95.2% and 97.8%. The stent with seven struts causes a reduction between 92.3% and 96.6%. The five and seven strut stents have the same effect on the path length reduction. The path length and the slope of the curves decrease with the number of struts, as

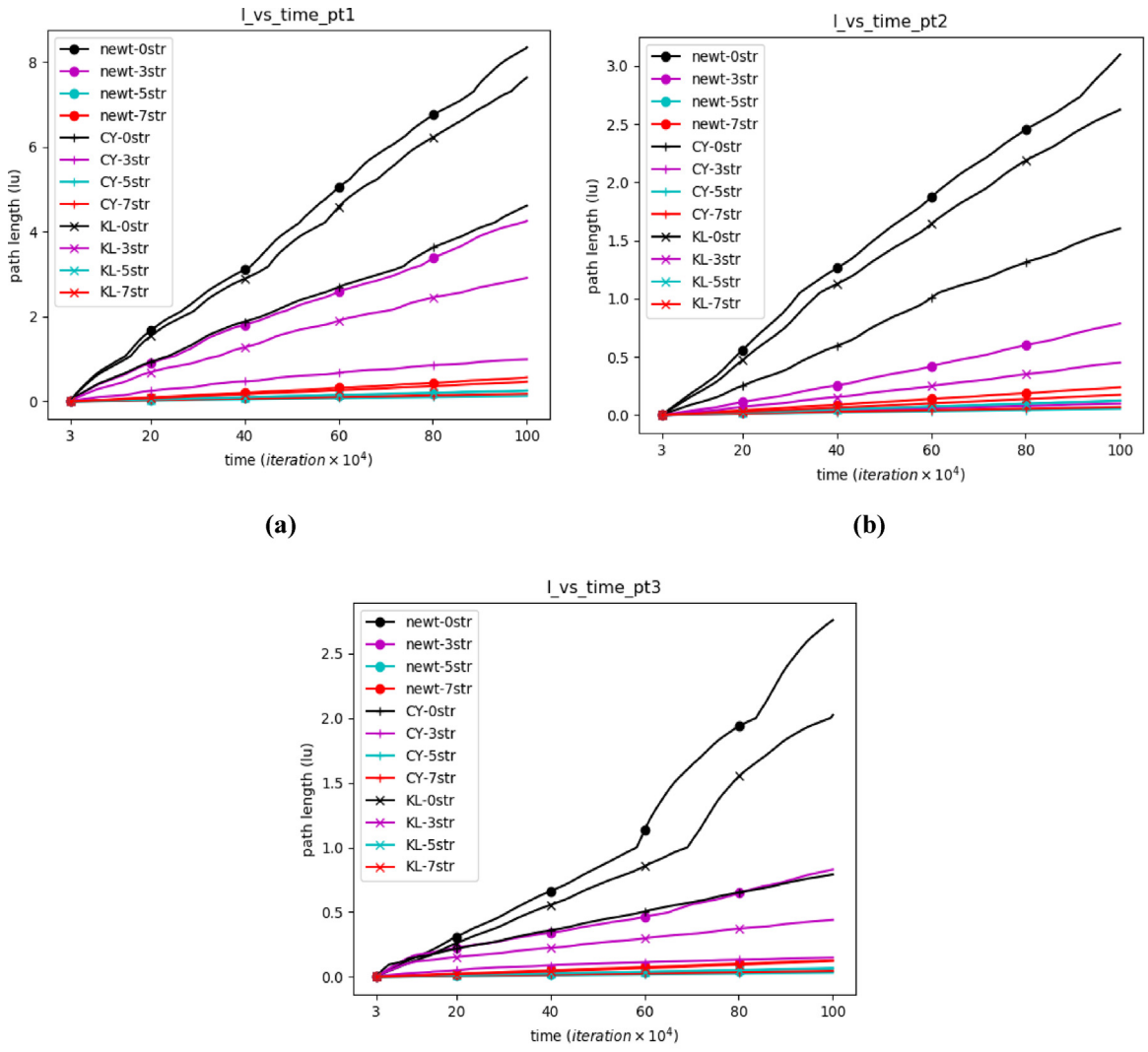

Fig. 11. Path length accomplished by particles fluids of points pt_1, pt_2, pt_3 inside the sac in (lu) according to struts number and rheological model. (a) Pt_1: pos_x(pt1) = 130, pos_y(pt1) = 70; (b) Pt_2: pos_x(pt2) = 184, pos_y(pt2) = 70; (c) Pt_3 : pos_x(pt3) = 157, pos_y(pt3) = 89.

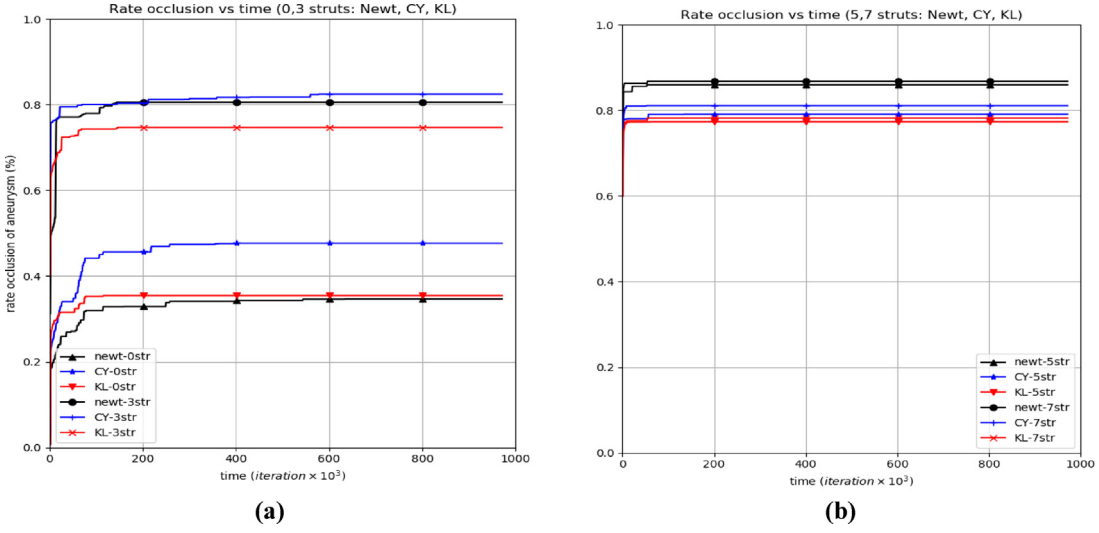

Fig. 12. Rate occlusion of aneurysm according to the number of struts and rheological behavior. (a) rate occlusion of the stent with (0, 3 struts); (b) rate occlusion of the stent with (5, 7 struts).

Fig. 13. Progression of thrombose generation in the aneurysmal sac predicted by Newtonian rheology behavior. (a) Free thrombosis generation; (b) stent with three struts; (c) stent with five struts; (d) stent with seven struts.

shown in Fig. 11, which means that the acceleration decreases and the fluid occupy small space for a long enough time.

The differences do not exceed 10%, and for the cases of low porosity stents (5 and 7 struts) the Newtonian model overestimates -slightly- the volume of the thrombosis (from 6.6 to 10%). However, the models give similar results regarding the estimation of thrombosis.

It should be noted that the thrombosis estimation model is fast and straightforward and does not require additional calculation apart from the hemodynamic calculation. It can be considered a quickly qualitative estimate model of the clot, which gives a general idea of the efficiency of the stent.

5. Conclusion

This work aims to conduct a numerical investigation of the hemodynamic effect of the treatment by stent of an intracranial aneurysm. A numeric code based on the lattice Boltzmann method has been developed and applied. Three numerical models have been used: Newtonian and non-Newtonian rheological behaviors (Carreau-Yasuda and K-L). The main findings obtained in the study are listed below.

- The intensity of the aneurysmal vortex decreases after placing a stent to the disappearance of the stent with seven struts (low porosity stent).
- The velocity, shear rate, and shear stress parameters decrease with increasing the number of stent struts.
- No need to go beyond porosity of 80% with five struts.
- The Newtonian model overestimates the distance traveled compared to the K-L and C-Y models.
- The three models give similar results regarding the velocity and the shear rate (the differences do not exceed 40%). As for the shear stress and path length, the three models give differences that reach 690%. This suggests that using non-Newtonian models is imperative when dealing with the hemodynamic aspect.
- Regarding the thrombose generation, the estimation of the occlusion rate by the three rheological models proposed differs little (2.4% and 10%) for the cases of stented aneurysms. In practice, it can be said that these differences are not significant, and the models can be used indifferently if the objective is the estimation of the rate occlusion

Declaration of Competing Interest

The authors declare no conflicts of interest with respect to the research, authorship and publication of this article.

References

[1] N. Etminan, G. Rinkel, Unruptured intracranial aneurysms: development, rupture and preventive management, Nat Rev Neurol 12 (2016) 699–713.
[2] R. Christoph, et al., Investigation of the velocity field in a full-scale model of a cerebral aneurysm, International Journal of Heat and Fluid Flow 43 (2013) 212–219.
[3] Joshua D. Hughes, K.M.B. Rania, A. Mekary, Michael C. Dewan, Abbas Rattani, Ronnie Baticulon, Yoko Kato, Hildo Azevedo-Filho, Jacques J. Morcos, Kee B. Park, Estimating the Global Incidence of Aneurysmal Subarachnoid Hemorrhage: A Systematic Review for Central Nervous System Vascular Lesions and Meta-Analysis of Ruptured Aneurysms, World Neurosurgery (2018) 430–447.e7.
[4] D. Nieuwkamp, et al., Changes in case fatality of aneurysmal subarachnoid haemorrhage over time, according to age, sex, and region: a meta-analysis, Lancet Neurol 8 (7) (2009) 635–642.
[5] A. Adamou, et al., Endovascular Treatment of Intracranial Aneurysms, Life 11 (4) (2021) 335.
[6] B.P. Catarina, S.M. Humberto, Clipping versus Coiling for Intracranial Aneurysms: Recent Trends, Journal of Anesthesia & Clinical Research 8 (6) (2017).
[7] Francesco Briganti, G.L. Mariano Marseglia, Giuseppe Mariniello, Ferdinando Caranci, Arturo Brunetti, Francesco Maiuri, Endovascular treatment of cerebral aneurysms using flow-diverter devices: A systematic review, Neuroradiol J 28 (4) (2015) 365–375.
[8] B. Chopard, R. Ouared, D.A. Rüfenacht, A lattice Boltzmann simulation of clotting in stented aneursysms and comparison with velocity or shear rate reductions, J Math. Comput. Simul. 72 (2006) 108–112.
[9] V.L. RAYZ, et al., Flow Residence Time and Regions of Intraluminal Thrombus Deposition in Intracranial Aneurysms, Annals of Biomedical Engineering 38 (10) (2010) 3058–3069.
[10] H.K. YONG, X. XIAOFENG, S.L. JOON, The Effect of Stent Porosity and Strut Shape on Saccular Aneurysm and its Numerical Analysis with Lattice Boltzmann Method, Annals of Biomedical Engineering 38 (7) (2010) 2274–2292.
[11] B.L. BARUCH, et al., Alteration of Hemodynamics in Aneurysm Models by Stenting: Influence of Stent Porosity, Annals of Biomedical Engineering 25 (1997) 460–469.
[12] R. Ouared, et al., Thrombosis modeling in intracranial aneurysms: a lattice Boltzmann, Computer Physics Communications 179 (2008) 128–131.
[13] M.N. Ngoepe, et al., Thrombosis in Cerebral Aneurysms and the Computational Modeling Thereof: A Review, Front Physiol. 9 (2018) (1664-042X (Print)).
[14] K. Zsolt, et al., Flow diversion treatment: intra-aneurismal blood flow velocity and WSS reduction are parameters to predict aneurysm thrombosis, Acta Neurochir, Springer-Verlag, 2012.
[15] M. Hirabayashi, et al., Characterization of flow reduction properties in an aneurysm due to a stent, Phys Rev E Stat Nonlin Soft Matter Phys. 68 (2 Pt 1) (2003).
[16] Y. Kim, X. Xu, J. Lee, The effect of stent porosity and strut shape on saccular aneurysm and its numerical analysis with lattice Boltzmann method, Annals of Biomedical Engineering 38 (7) (2010) 2274–2292.
[17] M.N. Ngoepe, Y. Ventikos, Computational modelling of clot development in patient-specific cerebral aneurysm cases, J Thromb Haemost 14 (2016) 262–272 (1538-7836 (Electronic)).
[18] J Jesty, Y.W. Perrotta P, D. Bluestein, Platelet activation in a circulating flow loop: combined effects of shear stress and exposure time, Platelets 14 (3) (2003) 143–149.
[19] M.C. Sukop, D.T. Thorne, Lattice Boltzmann Modeling: An Introduction for Geoscientists and Engineers, Springer, 2006.
[20] G. Zhaoli, S. Chang, Lattice Boltzmann Method and Its Applications in Engineering, Advances in Computational Fluid Dynamics, 420, World Scientific, 2013.
[21] T. Krüger, et al., The Lattice Boltzmann Method, in: Graduate Texts in Physics, Springer, 2017, p. 694. Cham. XXIV.

[22] F. Yilmaz, M.Y. Gundogdu, A critical review on blood flow in large arteries; relevance to blood rheology, viscosity models, and physiologic conditions, Korea-Australia Rheology Journal, 20 (4) (2008) 197–211.
[23] S.-W. Lee, On the effect of shear-thinning rheology on hemodynamic characteristics in basilar tip aneurysms with implication of two distinct flow patterns, Journal of Mechanical Science and Technology 26 (10) (2012) 3125–3132.
[24] S. Frolov, et al., Newtonian And Non-Newtonian Blood Flow At A 90 Degrees-Bifurcation Of The Cerebral Artery: A Comparative Study Of Fluid Viscosity Models, Journal of Mechanics in Medicine and Biology (5) (2018).
[25] H. Liu, et al., Comparison of Newtonian and Non-newtonian Fluid Models in Blood Flow Simulation in Patients With Intracranial Arterial Stenosis, Frontiers in Physiology 12 (2021).
[26] W. Chen-Hao, H. Jeng-Rong, A lattice Boltzmann approach for the non-Newtonian effect in the blood flow, Computers and Mathematics with Applications 62 (2011) 75–86.
[27] F. Irgens, Rheology and Non-Newtonian Fluids, Springer International Publishing Switzerland, 2014.
[28] B. Joshua, M.B. James, S. Green, Analysis of the Casson and Carreau-Yasuda non-Newtonian blood models in steady and oscillatory flows using the lattice Boltzmann method, Phys. Fluids 19 (2007) 093–103 19.
[29] K. Safoora, et al., Effect of rheological models on the hemodynamics within human aorta: CFD study on CT image-based geometry, Journal of Non-Newtonian Fluid Mechanics 207 (2014) 42–52.
[30] X.Y. Luo, Z.B. Kuang, A study on the constitutive equation of blood, J. Biomechanics, 25 (8) (1992) 929–934.
[31] J.-B. Zhang, Z.-B. Kuang, Study on blood constitutive parameters in di!erent blood constitutive equations, Journal of Biomechanics 33 (2000) 355–360.
[32] H.H. Afrouzi, et al., Simulation of blood flow in arteries with aneurysm: Lattice Boltzmann Approach (LBM), Comput Methods Programs Biomed 187 (2020) 105312.
[33] Y. Zare, S.P. Park, K.Y. Rhee, Analysis of complex viscosity and shear thinning behavior in poly (lactic acid)/poly (ethylene oxide)/carbon nanotubes biosensor based on Carreau–Yasuda model, Results in Physics 13 (2019) 102245.
[34] M. Junk, Z. Yang, Outflow boundary conditions for the lattice Boltzmann method, Progress in Computational Fluid Dynamics 8 (1-4) (2008) 38–48.
[35] R. Haimes, Using Residence Time for the Extraction of Recirculation Regions, American Institute of Aeronautics & AStronautics (1999).
[36] J. Bernsdorf, et al., Applying the lattice Boltzmann technique to biofluids: A novel approach to simulate blood coagulation, Computers and Mathematics with Applications 55 (2008) 1408–1414.
[37] M.J. Kunov, D.A. Steinman, C.R. Ethier, Particle Volumetric Residence Time Calculations in Arterial Geometries, ASME. J Biomech Eng. 118 (2) (1996) 158–164.
[38] B. Chopard, et al., Lattice Boltzmann Modeling of Thrombosis in Giant Aneurysms, INTERNATIONAL JOURNAL OF MODERN PHYSICS C 18 (4) (2007) 712–721.
[39] M.N. Ngoepe, et al., Thrombin-Fibrinogen In Vitro Flow Model of Thrombus Growth in Cerebral Aneurysms, TH open: companion journal to thrombosis and haemostasis 5 (2) (2021) e155–e162.
[40] G. Toth, R. Cerejo, Intracranial aneurysms: Review of current science and management, Vasc Med 23 (3) (2018) 276–288.
[41] Y. Zheng, et al., Size, Aspect Ratio and Anatomic Location of Ruptured Intracranial Aneurysms: Consecutive Series of 415 Patients from a Prospective, Multicenter, Observational Study, Cell Transplantation (2019) 739–746.
[42] R. Enzmann, et al., Blood Flow in Major Cerebral Arteries Measured by Phase–Contrast Cine MR, AJNR Am J Neuroradiol (15) (1994) 123–129.
[43] M.S. Charles, B.G. Virgil, R. Alan, Aneurysm Hemodynamics: An Experimental Study, AJNR Am J Neuroradiol 13 (4) (1992) 1089–1095.
[44] D. Ribeiro de Sousa, et al., Determination of a shear rate threshold for thrombus formation in intracranial aneurysms, J Neurointerv Surg 8 (8) (2016) 853–858.
[45] K. Baráth, et al., Influence of stent properties on the alteration of cerebral intra-aneurysmal haemodynamics: flow quantification in elastic sidewall aneurysm models, Neurological Research 27 (Suppl 1) (2005) S120–S128.
[46] O.C. Siobhan, W. Michael, M. Timothy, Numerical modelling of Newtonian and non-Newtonian representation of blood in a distal end-to-side vascular bypass graft anastomosis, Medical Engineering & Physics 28 (2006) 70–74.
[47] T. Cheng, D. Michel, PULSATILE FLOW OF NON-NEWTONIAN FLUIDS THROUGH ARTERIAL STENOSES, J. Biomechanics 29 (7) (1996) 899–908.
[48] S. Sandeep, S.R. Shine, Effect of stenosis and dilatation on the hemodynamic parameters associated with left coronary artery, Computer Methods and Programs in Biomedicine 204 (2021) 106052.
[49] C. Jie, L. Xi-Yun, Numerical investigation of the non-Newtonian blood flow in a bifurcation model with a non-planar branch, Journal of Biomechanics 37 (2004) 1899–1911.
[50] H. Kim, et al., Thrombosis and Recanalization of Small Saccular Cerebral Aneurysm: Two Case Reports and a Suggestion for Possible Mechanism, J Korean Neurosurg Soc 55 (5) (2014) 280–283.
[51] Y. Katayama, et al., Growth of totally thrombosed giant aneurysm within the posterior cranial fossa. Diagnostic and therapeutic considerations, Neuroradiology 33 (2) (1991) 168–170.